ARCHIVES OF ELECTRICAL ENGINEERING VOL. 65(2), pp. 327-336 (2016)

DOI 10.1515/aee-2016-0024

Recent simulation results of the magnetic induction tomography forward problem

KRZYSZTOF STAWICKI, BEATA SZUFLITOWSKA, MARCIN ZIOLKOWSKI

Department of Electrical and Computer Engineering
West Pomeranian University of Technology in Szczecin
70-313 Szczecin, Poland
e-mail: ks@zut.edu.pl

(Received: 10.06.2015, revised: 29.01.2016)

Abstract: In this paper we present the results of simulations of the Magnetic Induction Tomography (MIT) forward problem. Two complementary calculation techniques have been implemented and coupled, namely: the finite element method (applied in commercial software Comsol Multiphysics) and the second, algebraic manipulations on basic relationships of electromagnetism in Matlab. The developed combination saves a lot of time and makes a better use of the available computer resources.

Key words: boundary conditions, eddy current testing, finite element method, magnetic induction tomography.

1. Introduction

The Magnetic Induction Tomography (MIT) system has been developed and constructed at the West Pomeranian University of Technology, Szczecin for the inspection of low conductivity objects. Such objects can usually contain inclusions of different electromagnetic properties, i.e.: electrical conductivity σ (usually a few S/m), electrical permittivity ε [F/m] and magnetic permeability μ [H/m].

One of the highly promising MIT application is a biomedical diagnosis, because electrical properties of biological tissues are known to be sensitive to their physiological and pathological conditions. For example, it has been reported in the literature (see Table 1) that cancerous tissue has a meaningfully higher electrical conductivity than the surrounding tissues. Differences in electromagnetic properties values between various types of tissues (e.g. healthy and cancerous cells) are much more significant in comparison to other parameters, such as, for example density.

Table 1. The electric properties of normal and cancerous human hepatic tissue

Freq. [kHz]	Conductivity σ [mS/m]		Relative permittivity ε_r		$\omega\varepsilon$ [mS/m]		Loss tangent tgδ		Ref.
	Normal	Tumor	Normal	Tumor	Normal	Tumor	Norm	Tumor	
10.00	50 ± 22	296 ± 123	$(47 \pm 15)\cdot10^3$	$(50 \pm 15)\cdot10^3$	26.1 ±8.3	27.8 ± 8.3	1.91	10.65	[7]
10.00	42 ± 10	181 ± 80	$(35 \pm 8)\cdot10^3$	$(34 \pm 10)\cdot10^3$	19.4 ±4.5	18.9 ± 5.6	2.16	9.58	[8]
10.00	53.5	–	$28.9\cdot10^3$	–	16	–	3.33	–	[11]
15.63	47 ± 10	185 ± 80	$(28 \pm 7)\cdot10^3$	$(25 \pm 7)\cdot10^3$	24.3 ±6.1	21.7 ± 6.1	1.93	8.52	[9, 10]
15.63	58.0	–	$21.7\cdot10^3$	–	18.8	–	3.07	–	[11]
31.25	58 ± 20	195 ± 70	$(20 \pm 5)\cdot10^3$	$(16 \pm 5)\cdot10^3$	34.7 ±8.7	27.8 ± 8.6	1.67	7.01	[9, 10]
31.25	65.9	–	$14.0\cdot10^3$	–	24.3	–	2.71	–	[11]
65.10	76 ± 20	209 ± 70	$(13 \pm 3)\cdot10^3$	$(10 \pm 3)\cdot10^3$	47.1 ±1.1	36.1 ± 10.9	1.61	5.78	[9, 10]
97.66	91 ± 20	222 ± 70	$(11 \pm 2)\cdot10$	$(8.6 \pm 2)\cdot10^3$	59.7 ±1.1	46.7 ± 10.9	1.52	4.75	[9, 10]
100.0	109 ± 34	347 ± 126	$(13 \pm 3.8)\cdot10^3$	$(9.4\pm3.8)\cdot10^3$	72.3 ±21.1	52.3 ± 21.1	1.51	6.63	[7]
150.0	95.4	–	$6.09\cdot10^3$	–	50.8	–	1.88	–	[11]
195.3	124 ± 30	246 ± 70	$(6.5 \pm 1)\cdot10^3$	$(5.1 \pm 1)\cdot10^3$	70.5 ±10.8	55.3 ± 10.9	1.76	4.45	[9-11]
200.0	105	–	$5.20\cdot10^3$	–	57.8	–	1.82	–	[11]
300.0	122	–	$4.03\cdot10^3$	–	67.2	–	1.81	–	[11]
390.6	164 ± 30	272 ± 70	$(3.4 \pm 0.5)\cdot10^3$	$(3 \pm 0.6)\cdot10^3$	73.8 ±10.9	65.2 ± 13.0	2.22	4.17	[9, 10]
400.0	190 ± 56	399 ± 130	$(4.5 \pm 1.1)\cdot10^3$	$(3.2\pm1.6)\cdot10^3$	100 ±24.5	71.1 ± 35.6	1.90	5.61	[7]

2. The principle of the measuring system

The MIT system consists of two main elements, which are usually placed coaxially to each other, i.e.: a magnetic field exciter (ferrite core coil with an aluminium screen [4]) and a receiver (two differentially connected air core coils). The object under test is situated between them and during the measurements moves along the selected direction (Fig. 1). The remaining components of the system (signal generator with a high speed amplifier, control unit, data acquisition unit and a positioning system), though important, are not considered in the simulations.

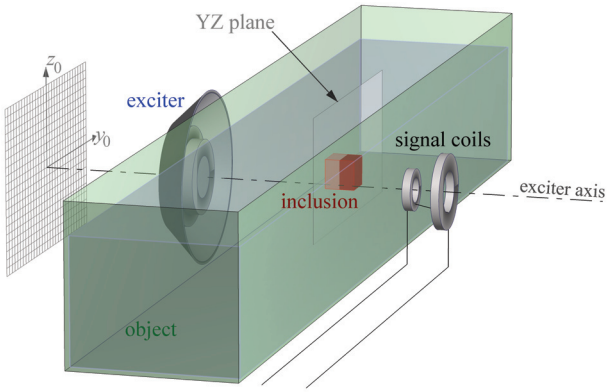

Fig. 1. Magnetic Induction Tomography system with a rectangular shaped object and an inclusion. The exciter and coaxial signal coils are coupled together and moves along the surface of the object

The exciter's coil is supplied by a low frequency sinusoidal current (of the order of tens of kilohertz) with an amplitude of tens of milliamperes and generates a time varying magnetic field, of the same frequency, described by magnetic flux density $\boldsymbol{B}_p$ and magnetic vector potential $\boldsymbol{A}_p$. This field, called the primary magnetic field, excites eddy currents in the conducting object. The amplitudes and spatial distribution of eddy currents vary depending on conductivities and shapes of the object and inclusions. Eddy currents create their own magnetic field, called the secondary field, which is described by magnetic flux density $\boldsymbol{B}_s$. The main aim of the measuring MIT system is to acquire the secondary magnetic field changes resulting from non-uniform electrical conductivity distribution in the object. The results of the secondary field measurements have been presented previously [3, 4].

The numerical modelling of such a process is commonly called the "forward problem". Next, the so called "inverse problem" takes places, i.e. reconstruction of the conductivity distribution based on the secondary magnetic field measurements.

3. Numerical model of the MIT system

The continuity equation for current density $\boldsymbol{J}$ varying sinusoidally with radial frequency ω, is given by:

$$\nabla \cdot \boldsymbol{J} = -\mathrm{j}\omega p\,, \tag{1}$$

where ρ is the charge density and the letter j denotes the imaginary unit. Substituting in this equation: from Ohm's law – conductivity σ multiplied by electric field vector $\boldsymbol{E}$ instead of current density ($\boldsymbol{J} = \sigma\boldsymbol{E}$), from Gauss's law – the divergence of electric displacement $\boldsymbol{D}$ instead of volume charge density ρ ($\nabla\cdot\boldsymbol{D} = \rho$) and using the relationship between displacement field $\boldsymbol{D}$ and electric field $\boldsymbol{E}$ ($\boldsymbol{D} = \varepsilon\boldsymbol{E}$), one can obtain the equation:

$$\nabla \cdot \left[(\sigma + \mathrm{j}\omega\varepsilon)\boldsymbol{E}\right] = 0\,. \tag{2}$$

In a linear isotropic nonmagnetic conductive medium the electric field can be expressed in terms of magnetic vector potential $\boldsymbol{A}$ and electric scalar potential Φ. For sinusoidally varying electromagnetic fields it can be written as:

$$\boldsymbol{E} = -\mathrm{j}\omega\boldsymbol{A} - \nabla\Phi\,, \tag{3}$$

From (2) and (3), if Coulomb's gauge $\nabla \cdot \boldsymbol{A} = 0$ is adopted, one can obtain:

$$\nabla \cdot \left[(\sigma + \mathrm{j}\omega\varepsilon)\nabla\Phi\right] = -\mathrm{j}\omega\boldsymbol{A} \cdot \nabla(\sigma + \mathrm{j}\omega\varepsilon)\,. \tag{4}$$

On the internal boundary between two different materials of parameters (σ_1, ε_1) and (σ_2, ε_2), the continuity condition for the electric field vectors is:

$$(\sigma_1 + \mathrm{j}\omega\varepsilon_1)E_{1n} = (\sigma_2 + \mathrm{j}\omega\varepsilon_2)E_{2n}\,, \tag{5}$$

where index n denotes the normal component of the vector. In the following, we will consider situations where the displacement current is negligible compared to the conduction current. It means that $\omega\varepsilon \ll \sigma$. This assumption is usually satisfied in most practical applications. In that case using (3), the reformulated problem (4)-(5) appears as:

$$\nabla \cdot (\sigma \nabla \Phi) = -\mathrm{j}\omega \boldsymbol{A} \cdot \nabla \sigma \,, \tag{6}$$

$$\sigma_1 \left(\frac{\partial \Phi_1}{\partial n} + \mathrm{j}\omega A_{1n} \right) = \left(\frac{\partial \Phi_2}{\partial n} + \mathrm{j}\omega A_{2n} \right). \tag{7}$$

The boundary condition on the object external boundaries one can obtain assuming $\sigma_2 = 0$, and taking σ and Φ in place of σ_1 and Φ_1:

$$\sigma \frac{\partial \Phi}{\partial n} = -\mathrm{j}\omega\sigma A_n \,. \tag{8}$$

The above partial differential equation and boundary conditions (6-8) describe general electromagnetic relations in the MIT system. There are two unknowns, namely: magnetic vector potential $\boldsymbol{A}$ and electric scalar potential Φ, which are in general both complex. The problem of solving the equations can be greatly simplified by the assumption that the primary magnetic vector potential $\boldsymbol{A}_p$ coming from the exciter is not disturbed by the object of low conductivity. The validity of this assumption for low frequencies, i.e. frequencies of the order of tens of kHz, is shown in [6]. The primary magnetic field can be calculated for a given exciter independently of the object parameters, and then $\boldsymbol{A} = \boldsymbol{A_p}$ can be considered as a known value in Equations (6-8).

Another simplification can be done by decomposing complex electric scalar potential Φ into real and imaginary parts $(\Phi = \Phi_r + \mathrm{j}\Phi_i)$. It was also shown in [6] that the real part of the potential is equal to zero. Substituting $\mathrm{j}\Phi_i$ into equations makes it possible to omit the j term in the both sides of all equations.

The primary magnetic vector potential $\boldsymbol{A}_p$ is the same at the interface between two different media, and therefore it is not necessary to use different notation for $\boldsymbol{A}_p$ on the right and left-hand side in (7). Finally, the reformulated problem (6-8) is reduced to finding one scalar function Φ_i from the set of equations:

$$\nabla \cdot (\sigma \nabla \Phi_i) = -\omega \boldsymbol{A}_p \cdot \nabla \sigma \,, \tag{9}$$

$$(\sigma_1 \Phi_i - \sigma_2 \nabla \Phi_i) \cdot \boldsymbol{n} = -\omega A_{pn} (\sigma_1 - \sigma_2) \,, \tag{10}$$

$$(\sigma \nabla \Phi_i) \cdot \boldsymbol{n} = -\omega\sigma A_{pn} \,. \tag{11}$$

4. The method for solving the forward problem

The whole measuring system can be simulated as one unified model in any finite element method (FEM) software taking into account the equation formulations (6-8) for the magnetic vector potential $\boldsymbol{A}$, and electric scalar potential Φ. However, in the case of complex 3D geo-

metry such an approach requires huge computer resources (memory and time). In this paper we describe the alternative method which is based on dividing the above complex computation process into smaller consecutive parts.

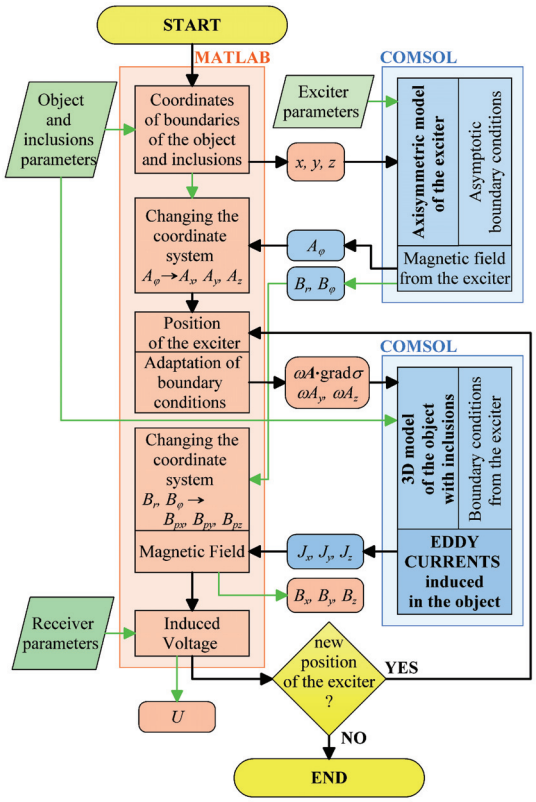

Fig. 2. Flowchart of the calculation procedure

First, the magnetic field $\boldsymbol{A}_p$ of the exciter is computed in the axisymmetric FEM model. The model does not contain the object, only the exciter. It is composed of the exciting coil of a rectangular cross section together with a ferromagnetic core and a conducting screen that have a slightly more complex shape. Because of the symmetry, there is only one component $A_\varphi(r, \varphi)$ of the magnetic vector potential, which has to be found from the equation:

$$\left(\mathrm{j}\omega\sigma - \omega^2\varepsilon_0\varepsilon_r\right)A_\varphi + \nabla\times\left(\mu_0^{-1}\mu_r^{-1}\boldsymbol{B}_p\right) = J_e\,, \tag{12}$$

where J_e is the current density in the exciter coil, σ is the conductivity of the screen, μ_r and μ_0 are the relative permeability of the core and the permeability of the vacuum. Asymptotic boundary conditions [5] adopted at the outer boundary of the model and 2D space of calculation enable to use extremely fine mesh and obtain accurate values of the field in a limited space. The calculated values of the magnetic field are converted into the Cartesian coordinate

system. They are saved and then can be used for succeeding calculation with any object, and with various receivers.

In the second step, from the values of the primary magnetic field and parameters of the object and inclusions (conductivities, positions and shapes), right hand side of Eq. (9) and boundary conditions at the edges of the object and inclusions – right hand side of Eq. (10) and (11) – are calculated. Next, these values are applied in the 3D FEM model (electric scalar potential Φ formulation). The model contains only the object with inclusions inside. A reduced number of algebraic equations allows for the use of the extra fine mesh and to compute accurately induced eddy currents. Finally, the secondary magnetic field and the electromotive force induced in receiver coils are calculated.

The second step can be repeated for different positions of the exciter. Moreover, calculation of voltages induced in the receiver coils can be done for various parameters of receivers. Both first and second steps of the calculations are made in smaller parts in Matlab and Comsol – see Fig 2 for details.

5. Equations in Comsol Multiphysics

The set of Equations (9-11) – partial differential equation and boundary conditions – has the form typical for electrostatics problems. This kind of problems can be solved by any commercial software. The software used in this work is Comsol Multiphysics. In AC/DC, 3D Electrostatics Module in this program one can find the following equations for domain and boundaries:

Space Charge Density (domain)

$$\nabla \cdot \boldsymbol{D} = \rho_v \,, \tag{13}$$

Surface Charge Density (interior boundary)

$$(\boldsymbol{D}_1 - \boldsymbol{D}_2) \cdot \boldsymbol{n} = \rho_s \,, \tag{14}$$

Surface Charge Density (exterior boundary)

$$-\boldsymbol{n} \cdot \boldsymbol{D} = \rho_s \,, \tag{15}$$

which can also be expressed in the forms similar to Equations (9-11):

$$\nabla \cdot (\varepsilon_0 \varepsilon_r \nabla V) = -\rho_v \,, \tag{13a}$$

$$(\varepsilon_0 \varepsilon_{r1} \nabla V - \varepsilon_0 \varepsilon_{r2} \nabla V) \cdot \boldsymbol{n} = -\rho_s \tag{14a}$$

$$\boldsymbol{n} \cdot (\varepsilon_0 \varepsilon_r \nabla V) = \rho_s \,. \tag{15a}$$

It can be seen that in (13a-15a) the term $\varepsilon_0 \varepsilon_r$ is equivalent to conductivity σ in (9-11) and V is the imaginary part of the electric scalar potential. The right hand side of both sets of

equations are functions of space and are known coefficients in all equations. After solving the problem, induced eddy currents can be calculated from the formula:

$$\boldsymbol{J} = -\mathrm{j}(\nabla V + \omega \boldsymbol{A}_p)\varepsilon_0 \varepsilon_r \,, \tag{16}$$

and the secondary magnetic field can be calculated from the Biot-Savart law.

6. Results of simulations

The validity of the model was examined using several examples. The first example is a conductive object (of size 0.12 × 1.19 × 0.2 m in x, y and z axis respectively and conductivity $\sigma = 0.145$ S/m) with a nonconductive inclusion (a cube with a 2 cm edge). The model was solved with the procedure described above, for 651 positions of the exciter (31 × 21 points in y_0z_0-plane, in which the exciter axis was placed – see Fig. 1). For every position of the exciter, eddy currents induced in the object were calculated from the FEM solution in 228480 evenly spaced points (the object is divided into cubes with a uniform current density). Figures 3-5 present components of induced current density in the YZ plane (part of the cross-section of the object, shown in Fig. 1). The component parallel to the exciter axis (J_x) exists only in close proximity of the inclusion or of the object boundary (the upper edge of each figure coincides with the boundary of the object).

Other components are continuous throughout the object, except the place where the inclusion is. It can be seen that the current flows around the inclusion and preserves continuity.

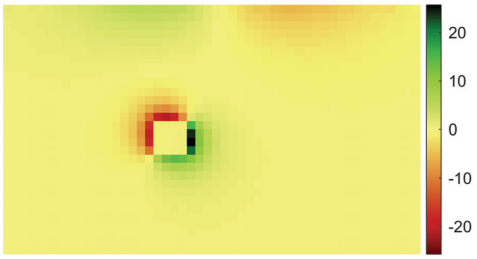

Fig. 3. J_x component of eddy currents density (mA/m^2) in the object with non-conductive inclusion

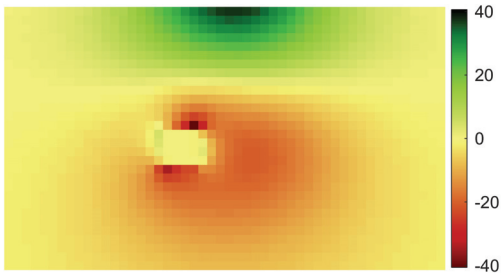

Fig. 4. J_y component of eddy currents density (mA/m^2) induced in the object with non-conductive inclusion

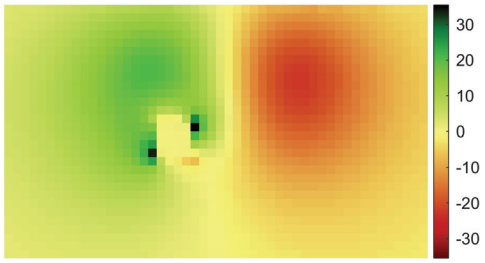

Fig. 5. J_z component of eddy currents density (mA/m^2) induced in the object with non-conductive inclusion

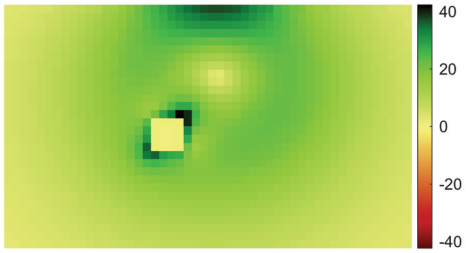

Fig. 6. Absolute value of eddy currents density (mA/m^2) induced in the object with non-conductive inclusion

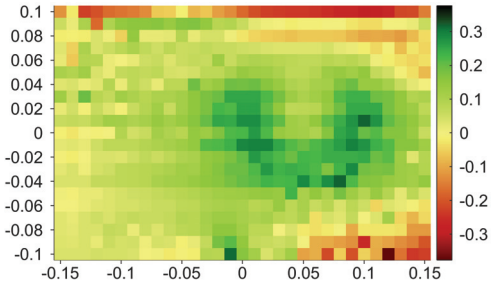

Fig. 7. Differential voltages U (mV) calculated for 651 positions (in y_0z_0-plane) of the exciter and receivers. The inclusion is placed at x = 0.02, y = 0.05, z = 0.02

Figure 6 presents the absolute value of the current density. Positions of the inclusion and the exciter axis can be seen very clearly. Figure 7 presents voltages calculated for every position of the exciter and receivers, for two differentially connected signal coils, as shown in Fig. 1. Although the inclusion is separated from the receiver by a relatively thick layer of a homogenous conductive object, it can be seen a signal produced by the inclusion.

Another example is an object with conductivity equal to the conductivity of a liver with a conductive inclusion inside. The liver is the biggest viscus in a human organism. Physiologically, about 75% of the livers blood supply comes from the portal vein, others – from the hepatic artery. Cancer cells are usually fed by branches of the hepatic artery. Hepatic tumors, benign and malignant, are richly vascularised and supplied with blood. It is estimated that the frequency of angiomas in the liver is 2-5% in general population and they are masses of

abnormal blood vessels. Angiomas, adenomas and others benign tumors could undergo to malignant transformation and cause haemorrhage. In the sonography it is extremely difficult to indentify small focal lesions in the liver. MIT can be employed in the detection of proliferative changes in the early stages. In medical imaging MIT is based on a higher value of electrical conductivity of blood, compared with most tissues. Eddy currents induced in the 3D heterogeneous model of an abdominal haemorrhage are shown in the Fig. 8, where the blood is the inclusion and the healthy tissue of the liver is the object. Slices are 1 mm and 1.5 mm away from the inclusion. In the top left corner of the figure induced current density is shown on a slice through the middle of the inclusion. It can be seen that induced currents are about six times bigger in the inclusion.

Table 2 presents the calculation time and physical memory usage, when computing the same object with different mesh parameters in two models: a full model of the MIT system and a reduced one. The reduced model consists only of the object and one inclusion and is solved only for the electric scalar potential (Eq. 9-11). The full model also includes the exciter and some space around, and is solved for both the electric scalar potential and the magnetic vector potential (Eq. 6-8). The calculation results are the same, but the number of degrees of freedom (NDF), the solution time and the physical memory usage are very different. In the most interesting case, for the finest mesh with the maximum element size in the object set to 6 mm in the domains and 2 mm on the boundaries, it was not possible to obtain the solution because of lack of memory.

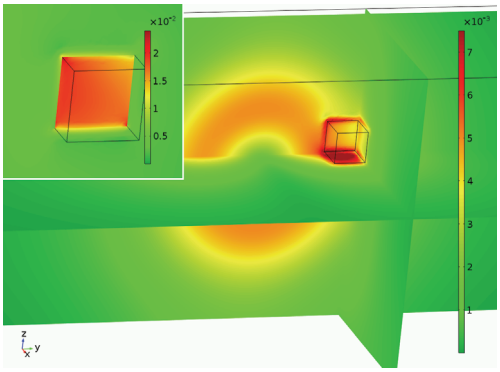

Fig. 8. Absolute value of eddy currents density (A/m^2) induced in the object (σ = 0.05 S/m) with inclusion of conductivity σ = 0.30 S/m

Table 2. The comparison of the calculation time and memory usage

Maximum element size		**NDF**		**solution time**		**RAM used**	
domains	boundaries	full model	reduced model	full model	reduced model	full model	reduced model
18 mm	6 mm	6053822	604825	34 min	70 s	29 GB	2.23 GB
12 mm	4 mm	13124483	1534537	65 min	121 s	60 GB	3.39 GB
6 mm	2 mm	58076408	7864656	n.a.	508 s	96 GB*	13.0 GB

* 96 GB is the total physical memory installed on the computer

7. Conclusions

The procedure for solving the forward problem for Magnetic Induction Tomography and simulation results that confirm the validity of the procedure were presented. The procedure is fast compared to traditional methods, it uses much less memory and can be used in designing similar measuring systems.

References

[1] Li X., Mariappan L., He B., *Three-Dimensional Multiexcitation Magnetoacoustic Tomography with Magnetic Induction*, Journal of Applied Physics 108, 124702 (2010).

[2] Surowiec A.J., Stuchly S.S., Barr J.R., Swarup A., *Dielectric properties of breast carcinoma and the surrounding tissues*, IEEE Transactions on Biomedical Engineering 35(4), 257263 (1988).

[3] Stawicki K., Gratkowski S., Komorowski M., Pietrusewicz T., *Numerical simulations and experimental results for magnetic induction tomography system*, Przegląd Elektrotechniczny 85(4): 44-46 (2009).

[4] Stawicki K., Gratkowski S., Komorowski M., Pietrusewicz T., *A New Transducer for Magnetic Induction Tomography*, IEEE Transactions on Magnetics 45(3), 1832-1835 (2009).

[5] Gratkowski S., Pichon L., Gajan H., *Asymptotic Boundary Conditions for Open Boundaries of Axisymmetric Magnetostatic Finite-Element Models*, IEEE Transactions on Magnetics 38(2): 469-472 (2002).

[6] Gencer N.G., Kuzuoglu M., Ider Y.Z., *Electrical Impedance Tomography Using Induced Currents*, IEEE Transactions on Medical Imaging 13(2): 338-350 (1994).

[7] Prakash S., Karnes M.P., Sequin E.K., West J.D. et al, *Ex vivo electrical impedance measurements on excised hepatic tissue from human patients with metastatic colorectal cancer*, Physiological Measurement 36: 315-328 (2015).

[8] Laufer S., Ivorra A., Reuter V.E., Rubinsky B., Solomon S., *Electrical impedance characterization of normal and cancerous human hepatic tissue*, Physiological Measurement 31: 995-1009 (2010).

[9] Gabriel S., Lau R.W. and Gabriel C., *The dielectric properties of biological tissues: II. Measurements in the frequency range 10 Hz to 20 GHz*, Physics in Medicine and Biology 41: 2251-69 (1996).

[10] Haemmerich D., Schutt D.J., Wright A.S., Webster J.G., Mahvi D.M., *Electrical conductivity measurement of excised human metastatic liver tumors before and after thermal ablation*, Physiological Measurement 30: 459-466 (2009).

[11] http://www.itis.ethz.ch/virtual-population/tissue-properties/database/dielectric-properties/, accessed July 2015.